J Physiol (2003), **550.3**, *pp.* 829–844
DOI: 10.1113/jphysiol.2003.042176

www.jphysiol.org

Journal of Physiology

Electrical coupling between the myenteric interstitial cells of Cajal and adjacent muscle layers in the guinea-pig gastric antrum

H. M. Cousins, F. R. Edwards, H. Hickey, C. E. Hill* and G. D. S. Hirst

*Department of Zoology, University of Melbourne, Victoria 3010 and *Division of Neuroscience, John Curtin School of Medical Research, Canberra, ACT, Australia*

Intracellular recordings were made from short segments of the muscular wall of the guinea-pig gastric antrum. Preparations were impaled using two independent microelectrodes, one positioned in the circular layer and the other either in the longitudinal layer, in the network of myenteric interstitial cells of Cajal (ICC_{MY}) or in the circular layer. Cells in each layer displayed characteristic patterns of rhythmical activity, with the largest signals being generated by ICC_{MY}. Current pulses injected into the circular muscle layer produced electrotonic potentials in each cell layer, indicating that the layers are electrically interconnected. The amplitudes of these electrotonic potentials were largest in the circular layer and smallest in the longitudinal layer. An analysis of electrical coupling between the three layers suggests that although the cells in each layer are well coupled to neighbouring cells, the coupling between either muscle layer and the network of ICC_{MY} is relatively poor. The electrical connections between ICC_{MY} and the circular layer did not rectify. In parallel immunohistochemical studies, the distribution of the connexins Cx40, Cx43 and Cx45 within the antral wall was determined. Only Cx43 was detected; it was widely distributed on ICC_{MY} and throughout the circular smooth muscle layer, being concentrated around ICC_{IM}, but was less abundant in the circular muscle layer immediately adjacent to ICC_{MY}. Although the electrophysiological studies indicate that smooth muscle cells in the longitudinal muscle layer are electrically coupled to each other, none of the connexins examined were detected in this layer.

(Received 23 February 2003; accepted after revision 28 April 2003; first published online 4 July 2003)
Corresponding author G .D. S. Hirst: Department of Zoology, University of Melbourne, Victoria 3010, Australia.
Email: d.hirst@zoology.unimelb.edu.au

The antral region of the stomach generates an ongoing discharge of slow waves. Slow waves in this and other regions of the gastrointestinal tract are initiated by a network of interstitial cells of Cajal (ICC), which most frequently lies near the myenteric plexus (ICC_{MY}; Sanders, 1996). Thus, intestinal tissues taken from mutant mice that lack ICC_{MY} fail to generate slow waves (Ward *et al.* 1994). Similarly, slow waves are not detected in gastric tissues in which the development of ICC_{MY} has been impaired (Ordog *et al.* 1999). ICC_{MY} in the gastric antrum of guinea-pig or mouse generate large-amplitude, long-lasting pacemaker potentials (Dickens *et al.* 1999; Hirst & Edwards, 2001; Hirst *et al.* 2002*a*). These potentials appear to spread passively to the circular muscle layer (Dickens *et al.* 1999) where each wave of depolarization triggers the secondary regenerative component of the slow wave (Ohba *et al.* 1975; Dickens *et al.* 1999; Edwards *et al.* 1999; Suzuki & Hirst, 1999; van Helden *et al.* 2000; Hirst *et al.* 2002*a*). The secondary regenerative component of the slow wave is initiated by a second population of intramuscular ICC (ICC_{IM}), which are distributed amongst the smooth muscle cells making up the circular layer (Burns *et al.* 1997). Thus, the second component of the slow wave is absent in mouse antral tissues that lack ICC_{IM} (Dickens *et al.* 2001; Hirst *et al.* 2002*a*). In the longitudinal layer, pacemaker potentials give rise to follower potentials, which lack secondary regenerative components (Hirst & Edwards, 2001).

In the heart, pacemaker cells are concentrated in the sinoatrial node, and pacemaker potentials conduct into nearby atrial cells. In contrast, the pacemaker cells of the gastric antrum, ICC_{MY}, form an extensive thin network lying between the longitudinal and circular layers (Burns *et al.* 1997; Hirst *et al.* 2002*a*). Clearly, if ICC_{MY} directly initiate slow waves in the circular layer and follower potentials in the longitudinal layer, they must be electrically connected to both layers. However, the connections must be such that the membrane potential of pacemaker cells is not dominated by those of the circular and longitudinal muscle layers, each of which are several cells thick. Moreover, the electrical network must have properties that allow the two muscle layers to generate distinct sequences of membrane potential changes during each slow-wave cycle (Dickens *et al.* 1999, 2000). The

initial series of experiments described in this report examined the properties of the electrical connections between the network of pacemaker cells and the adjacent muscle layers. These experiments were carried out on electrically small sections of gastric antrum that consisted of a layer of ICC_{MY} along with both the circular and longitudinal muscle layers. It was found that the coupling between ICC_{MY} and adjacent muscle cells was relatively poor, but was sufficient to allow an adequate flow of pacemaker current for the initiation of slow waves and follower potentials. Furthermore, the apparent dissociation of electrical activity detected in the longitudinal and circular muscle layers during each slow-wave cycle could be accounted for if the resistance of the layer of ICC_{MY} fell to a low value during each pacemaker potential. This fall in resistance reduced the transfer of signal between the two muscle layers, even though the coupling resistances remained unaltered. The second series of experiments made use of antibodies selective to the connexins Cx40, Cx43 and Cx45, in an attempt to determine whether the distribution of connexins was correlated to the pattern of electrical coupling detected between the different cell types.

METHODS

Electrophysiological methods

The procedures described herein were approved by the animal experimentation ethics committee at the University of Melbourne. Guinea-pigs of either sex were stunned, exsanguinated and the stomach removed. The antral region was isolated and immersed in oxygenated physiological saline (composition, mM): NaCl 120, $NaHCO_3$ 25, NaH_2PO_4 1.0 KCl 5, $MgCl_2$ 2, $CaCl_2$ 2.5 and glucose 11; bubbled with 95 % O_2 : 5 % CO_2. The mucosa was removed, followed by the serosa, and individual preparations consisting of a single bundle of circular muscle (diameter 60–150 μm, length 400–800 μm) with the adhering longitudinal layer were dissected free using a fragment of broken razor blade. Preparations were pinned, serosal surface uppermost, in a recording chamber that had a base consisting of a microscope coverslip coated with Sylgard silicone resin (Dow Corning, Midland, MI 48640, USA) and viewed with the aid of an inverted compound microscope. Preparations were impaled with two independently mounted, sharp electrodes, of resistance 120–160 MΩ and filled with 0.5 M KCl. One was pushed through the layers of longitudinal smooth muscle and ICC_{MY} and positioned in the circular layer, where slow waves were detected. The second was first positioned in the longitudinal layer so as to record follower potentials (Dickens *et al.* 1999). Current pulses were passed through the electrode positioned in the circular layer and the resulting electrotonic potential was recorded from the longitudinal layer. The second recording electrode was then advanced into a myenteric ICC, and pacemaker potentials were recorded. Current pulses were again passed through the electrode impaling a smooth muscle cell in the circular layer and the resulting electrotonic potentials were recorded from ICC_{MY}. Finally, the recording electrode was advanced into the circular layer and the electrotonic potentials generated by current pulses passed through the first electrode, which was impaled in the circular muscle layer, were recorded. Membrane potential changes and membrane currents were amplified using an Axoclamp-2B amplifier (Axon Instruments, Foster City, CA, USA), low-pass filtered (cut-off frequency, 100 Hz), digitized and stored on computer for later analysis. During each experiment, preparations were constantly superfused with physiological saline solution warmed to 37 °C; nifedipine (1 μM) was added to the physiological saline to reduce the amplitudes of the contractions associated with each slow wave. In initial experiments it was found that caffeine (1 mM), which suppresses the frequency of occurrence of unitary potentials (Edwards *et al.* 1999), so increasing the signal-to-noise ratio, had no effect on the amplitudes of the electrotonic potentials recorded in each layer. Hence, many electrotonic potentials were recorded in physiological saline containing caffeine.

All data are expressed as means ± S.E.M. Student's *t* test was used to determine if data sets differed, with $P < 0.05$ taken to indicate a significant difference. Caffeine and nifedipine (obtained from Sigma, St Louis, MO, USA) were used in these experiments.

Equivalent electrical circuit

If the circular muscle layer is considered to be isopotential, its steady-state behaviour can be modelled by a single resistor, R_C. Similarly, the network of ICC can be represented by a resistor, R_{ICC}, and the longitudinal muscle layer by R_L. The ICC_{MY} network is connected to the circular muscle layer by a resistance $R_{C–IC}$, and to the longitudinal muscle layer by a resistance $R_{L–IC}$ (Fig. 1*B*).

If current (I) is injected via a microelectrode into the circular muscle layer, voltages may be measured with a second microelectrode at the circular muscle layer (V_1), the ICC_{MY} layer (V_2) and the longitudinal muscle layer (V_3). Applying Kirchoff's current law (the net current into a node is zero) at each circuit node yields three equations. Subsequently, if the same current is injected into the longitudinal muscle layer and nodal voltages are again measured from the three layers, three further equations can be similarly constructed. Therefore, six equations are obtained in terms of the equivalent circuit's five unknown resistors. A least-squares solution of this overdetermined system of simultaneous equations can be found using direct methods based on Gaussian elimination (Matlab 6.0). However, this approach requires making a series of five successive pairs of impalements from a single preparation. This proved technically too difficult, and an alternative analysis was sought that was not dependent upon repeated measurements being made from the different cell layers during current injection into both the circular and longitudinal muscle layers. During spontaneous antral activity, the depolarization of the pacemaker potential in the ICC_{MY} layer can be measured (Fig. 1*C*; V_5), as can be the electrically coupled initial phase of the slow wave in the circular muscle layer (V_4). Application of caffeine abolishes the regenerative phase of the slow wave and leaves only the initial component (Dickens *et al.* 1999). These two voltage measurements allow calculation of the ratio of R_C to $R_{C–IC}$ without the need to impale a longitudinal muscle cell.

A simplifying restriction was introduced to reduce the number of unknown variables by one. If it is assumed that $R_{C–IC}$ and $R_{L–IC}$ have the same value, R_X, then the three equations obtained by current injection into the circular muscle, together with the ratio of R_C to $R_{C–IC}$ provide four simultaneous equations with four unknown variables. This approximation to the problem is then solvable by substitution.

Considering the experiment in which current is injected into the circular muscle layer (Fig. 1*B*), according to Ohm's law the ratio of two resistors carrying the same current is equal to the ratio of the voltages across them, giving:

$$\frac{R_L}{R_X} = \frac{V_3}{V_2 - V_3} \equiv L, \quad (1)$$

wherein L is defined as the ratio of R_L to R_X.

Similarly,

$$\frac{R_{ICC} \,||\, (R_X + R_L)}{R_X + R_{ICC} \,||\, (R_X + R_L)} = \frac{V_2}{V_1},$$

where '||' means 'in parallel with' so that

$$R_1 \,||\, R_2 = \frac{R_1 R_2}{R_1 + R_2}.$$

Expanding and gathering terms yields eqn (2), wherein J is defined as the ratio of R_{ICC} to R_X:

$$\frac{R_{ICC}}{R_X} = \frac{V_2(L+1)}{(V_1 - V_2)(L+1) - V_2} \equiv J \quad (2)$$

Considering the circular muscle node, a direct measure of input resistance of the network (R_{IN}) is available because V_1 and I are both known. The expression for the series–parallel combination of resistors seen from this node can also be constructed:

$$R_{IN} = \frac{V_1}{I} R_C \,||\, (R_X + R_{ICC} \,||\, (R_X + R_L))$$

Expanding this equation and gathering terms yields eqn (3):

$$R_X = \left(\frac{C+K}{CK}\right)\left(\frac{V_1}{I}\right), \quad \text{where } K = 1 + \frac{J(L+1)}{J+L+1}, \quad (3)$$

where C is the ratio of R_C to R_X. This ratio can be found by considering the circular muscle node during the plateau of a slow wave (Fig. 1*C*).

$$\frac{R_C}{R_X} = \frac{V_4}{V_5 - V_4} \equiv C, \quad (4)$$

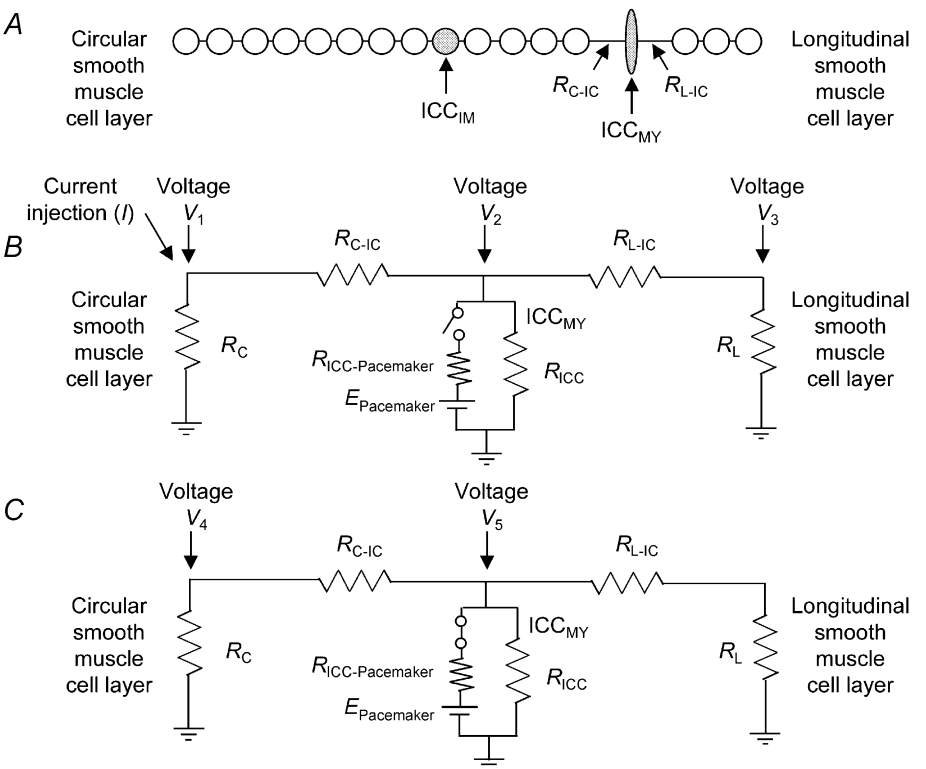

Figure 1. Equivalent electrical circuit of a short segment of the muscular wall of the gastric antrum

A, a schematic representation of a small segment of antral wall comprising a layer of circular smooth muscle, which includes some ICC_{IM}, connected via a resistive pathway (R_{C-IC}) to the ICC_{MY} layer. On the right of the panel, a layer of longitudinal smooth muscle is also connected to the ICC_{MY} layer via a resistive pathway (R_{L-IC}). *B*, the equivalent electrical circuit describing current injection (I) into a circular muscle cell. Shown are equivalent resistors for the circular layer (R_C), the ICC_{MY} layer (R_{ICC}) and the longitudinal layer (R_L). Access resistances connecting the ICC_{MY} to the muscle layers are shown as R_{C-IC} to the circular muscle layer and R_{L-IC}, to the longitudinal muscle layer. Steady-state voltages arising in response to current injection, V_1, V_2 and V_3, are marked at the circular, ICC_{MY} and longitudinal layers. Also shown are pacemaking elements, $R_{ICC-Pacemaker}$ and $E_{Pacemaker}$, but these are disconnected to simulate baseline conditions; their connecting switch is shown open. *C*, the equivalent circuit describing the state during spontaneous depolarization of the ICC_{MY} layer in the absence of current injection. In this case, depolarization (V_5) occurs because the switch is closed, mimicking the peak of a pacemaker potential. $R_{ICC-Pacemaker}$ represents the increase in ICC_{MY} membrane conductance that provides the pacemaker current shunt, and $E_{Pacemaker}$ represents the equilibrium potential for the pacemaker current.

Substituting C, J and L into eqn (3) yields a value for R_X. This value can be substituted into eqns (1), (2) and (4) to solve for R_L, R_{ICC} and R_C. The driving potential for the pacemaker current was assumed to be near the peak amplitude of a pacemaker potential (Hirst & Edwards, 2001).

Immunohistochemical methods

Segments of fresh antrum were impregnated with 30 % sucrose in phosphate-buffered saline (PBS) for 1 h and then transferred to a 1:1 mixture of OCT compound (Tissue Tek, Elkhart, IN, USA) and 30 % sucrose in PBS for 10 min prior to freezing in OCT. Transverse cryosections (10 μm thick) of the antrum were cut on a cryotome (Leica, Model Jung CM3000), either parallel or perpendicular to the circular muscle bundles, mounted on Superfrost slides (Menzel-Glaser, Germany)and then air dried. The relationship between ICC and connexins was determined using dual-labelling immunohistochemistry by consecutive incubation with antibodies to Cx43, Cx40 or Cx45 followed by incubation with an antibody to receptor tyrosine kinase (Kit; ACK2, Chemicon, Australia). Each cryosection was incubated at room temperature in a humidified chamber for 20 min in blocking solution (2 % bovine serum albumin with 0.2 % Triton X-100 in PBS) prior to incubation in primary antibody for 1 h with rabbit or sheep antibodies against Cx43, Cx40 and Cx45 (1:250; diluted in blocking solution). Sections were washed with PBS and then incubated in secondary antibody labelled with a fluorescent marker, either Alexa 488 goat anti-rabbit or donkey anti-sheep antibodies (1:250; Molecular Probes, Eugene, OR, USA) diluted in 0.01 % Triton X-100 in PBS, for 1 h. Subsequently, the cryosections were washed in PBS and incubated in Kit primary antibody (1:250, diluted in PBS) at room temperature for 30 min and then, following PBS washes, in a mouse anti-rat IgG antibody labelled with a fluorescent marker (IgG-Alexa 568, 1:250, Molecular Probes) for 30 min. Specimens were rinsed in PBS and mounted in mounting medium (Glycergel; Dako, CA, USA) for examination.

Antibodies

ICC were identified using ACK2, a rat monoclonal antibody that recognizes an extracellular domain of the protein c-Kit. Antibodies against Cx43 (Zymed, San Francisco, CA, USA) were raised in rabbits against a peptide contained in the C-terminal portion of the third cytoplasmic domain, its reactivity being independent of phosphorylation status. Anti-Cx40 was raised in sheep against a peptide corresponding to amino acids 254–270 of rat Cx40, and has been used in previous studies (Hill *et al.* 2002; Rummery *et al.* 2002). Antibodies against Cx45 were raised in sheep against a peptide corresponding to amino acids 354–367 of human Cx45, as described previously (Rummery *et al.* 2002). To test the specificity of the connexin staining observed, the primary connexin antibody was preincubated for 1 h at room temperature with a 20-fold excess by weight of the peptide against which the antibody was raised, before application to the cryosections. Immunostaining was not detected either in the absence of primary antibody or when the antibody was preincubated with the appropriate peptide. Parallel controls to test connexin antibody penetration and selectivity were carried out using rat tail artery, in which the endothelial cells are associated with Cx40 and Cx43, and rat endocardium (Cx40, Cx45), in which the specified connexins have been described previously (Coppen *et al.* 1998; Rummery *et al.* 2002). In each case, connexin immunostaining was observed in the positive control tissue.

Analysis

Cryostat sections were viewed with the aid of a microscope (Axioplan 2, Zeiss, Germany) fitted with a confocal laser scanning system (Biorad Microradiance, Hemel Hempstead, UK) equipped with helium–neon and argon laser sources. Single optical sections of 0.5 μm were made in the Z-axis, and Z-stacks were compiled. To determine the connexin labelling associated with ICC_{IM} or ICC_{MY} cells, colocalization maps of connexin and Kit staining were generated for each optical section using Biorad software (Lasersharp version 3.2). From these images, the percentage of cell surface area covered by connexin immunostaining was determined for Kit-positive cells using the grain-counting function of the Micro-Computer Image Device software program (MCID version 5, Imaging Research, Canada). The surface areas of these ICC_{IM} or ICC_{MY} cells were also determined from three-dimensional reconstructions from stacks of serial optical sections stained with the Kit antibody. From these measurements, the percentage of ICC_{IM} or ICC_{MY} membrane associated with connexin immunoreactivity was determined. For smooth muscle cells, connexin expression was quantified by calculating the area of Cx43 immunostaining in a known volume of antral circular muscle tissue devoid of Kit immunoreactivity. The number of smooth muscle cells within the measured volume of tissue examined was calculated assuming firstly that the smooth muscle cells had the dimensions determined previously (Dickens *et al.* 1999) and that the volume of extracellular space was negligible. This allowed an estimate of the area of Cx43 staining per muscle cell and hence an estimate of the percentage of circular smooth muscle cell surface area immunostained for any particular connexin subtype.

RESULTS

General observations

Intracellular recordings were made from small preparations of antral muscle wall, which consisted of a short length of a discrete bundle of circular muscle, with the network of ICC_{MY} and longitudinal muscle layer above that circular bundle remaining attached. Three distinct patterns of rhythmical electrical activity were recorded (Fig. 2). One electrode was pushed through the outer longitudinal muscle layer and the ICC_{MY} layer until a cell generating slow waves was impaled. The first type of cell that was encountered by the second electrode at the serosal surface generated follower potentials with properties similar to those described when recordings were made from anatomically identified longitudinal muscle cells (Fig. 2*A*; Dickens *et al.* 1999). Follower potentials had amplitudes in the range 9–31 mV (mean, 23.4 ± 2.0 mV, n = 12, where each n value represents a measurement from a separate preparation) and maximum rates of rise in the range 10–120 mV s^{-1} (65 ± 20 mV s^{-1}, n = 12); cells had peak negative potentials in the range −57 to −64 mV (−61.3 ± 0.6 mV, n = 12). In several preparations, follower potentials displayed prominent discharges of transient hyperpolarizing potentials, but never displayed discharges of unitary potentials (see Fig. 5*Ca*). After passing through the longitudinal layer, pacemaker potentials were detected (Fig. 2*B*) with properties similar to those described when recordings were made from anatomically identified ICC_{MY} (Dickens *et al.* 1999). Pacemaker potentials had amplitudes in the range 39.2–48.4 mV (42.7 ± 1.4 mV, n = 8) and maximum rates of rise in the range

300–860 mV s^{-1} (590 ± 80 mV s^{-1}, $n = 8$): cells had peak negative potentials in the range −59 to −70 mV (−63.9 ± 1.3 mV, $n = 8$). Unlike the recordings made from larger preparations, most pacemaker potentials recorded from the smaller preparations were preceded by a 'noisy' diastolic depolarization made up of unitary potentials (see Hirst & Edwards, 2001). Furthermore, in these small preparations pacemaker potentials were never followed by an afterdepolarization (see Hirst & Edwards, 2001). Presumably these differences occurred because in the small preparations used in this study, pacemaker potentials were invariably initiated electrically close to the recording point: they could neither be triggered at electrically distant points nor conduct through electrically distant regions, since these areas were removed in the dissection. The third type of cells, which were located below ICC_{MY}, generated slow waves, each of which had an initial passive component and a secondary regenerative component. In a given preparation, slow waves had identical time courses when detected by either electrode (Fig. 2*C*). Slow waves had peak amplitudes in the range 19.0–38.0 mV (31.4 ± 1.4 mV, $n = 14$), superimposed on peak negative potentials in the range −60 to −69 mV (−63.1 ± 0.7 mV, $n = 14$). Primary components had amplitudes in the range 12–32 mV (15.8 ± 1.6 mV, $n = 14$), with maximum rates of rise in the range 10–90 mV s^{-1} (40 ± 5 mV s^{-1}, $n = 14$). Slow waves occurred at a frequency of 2.5 ± 0.1 slow waves min^{-1} ($n = 14$). The amplitudes of the primary component of the slow wave differed significantly from those of follower potentials (see Figs 2, 5, 6 and 7).

When paired simultaneous recordings made from different cell types were examined, the waves of depolarization in each cell layer were found to occur synchronously, with activity being initiated by ICC_{MY} (Fig. 2; Dickens *et al.* 1999; Hirst & Edwards, 2001).

Electrical coupling between cells in the gastric antrum

When the preparations were impaled with two electrodes, hyperpolarizing current pulses that passed through one electrode in the interval between slow waves invariably evoked an electrotonic potential that was detected by the second electrode, regardless of which combination of cells was impaled. However, the amplitudes of the potentials generated by a given current pulse varied depending upon which combination of cells was impaled (Fig. 3*Aa*). When current was injected into the circular layer and the resultant electrotonic potential was recorded from the same layer, preparations had input resistances in the range 0.70–3.12 MΩ (1.52 ± 0.20 MΩ, $n = 14$). When current

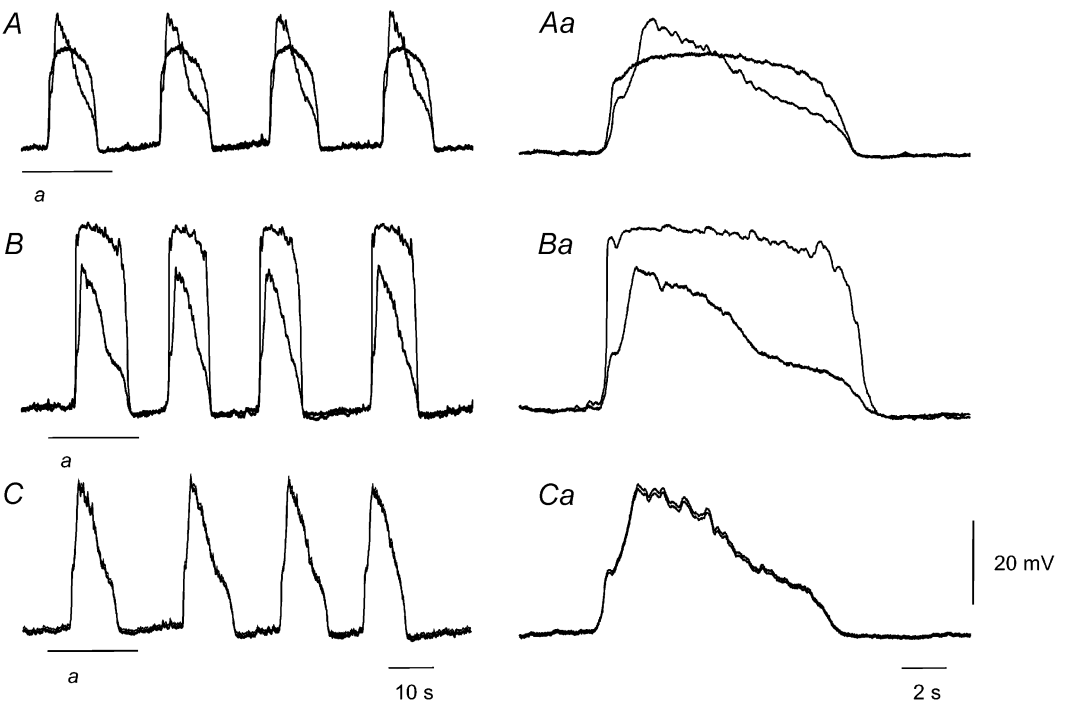

Figure 2. Paired intracellular recordings from different cells lying in the gastric antrum

A, a record from a circular muscle cell and a simultaneous record of smaller amplitude from a longitudinal muscle cell. *Aa*, part of the same record (indicated by a bar labelled *a* beneath the record) on an expanded time base. *B*, a record from a circular muscle cell and a simultaneous record of larger amplitude from an ICC_{MY}. *Ba*, the indicated part of the same record on an expanded time base. *C*, two simultaneous records from two independently impaled circular muscle cells. *Ca*, the indicated part of the same record on an expanded time base. The voltage and time calibration bars apply to all traces. The membrane potentials of the circular smooth muscle layer, ICC_{MY} and longitudinal layer were −62, −63 and −60 mV, respectively.

was injected into the circular layer and the resultant electrotonic potential was recorded from the layer of ICC_{MY}, preparations had transfer resistances in the range 0.54–1.21 MΩ (0.67 ± 0.09 MΩ, $n = 8$), with the transfer resistance being defined as the amplitude of the electrotonic potential detected in the ICC_{MY} divided by the amplitude of current injected into the circular layer. When current was injected into the circular layer and the resultant electrotonic potential was recorded from the longitudinal muscle layer, preparations had transfer resistances in the range 0.10–0.78 MΩ (0.41 ± 0.07 MΩ, $n = 12$), with the transfer resistance in this case being defined as the amplitude of the electrotonic potential detected in the longitudinal layer divided by the amplitude of current injected into the circular layer. Using an unpaired *t* test, the transfer resistances between ICC_{MY} and circular muscle were found to differ significantly from the corresponding input resistances of the circular muscle layer. Similarly, the transfer resistances between longitudinal muscle and circular muscle differed significantly from the input resistances at the circular muscle layer. Furthermore, the circular muscle-to-ICC_{MY} transfer resistances differed significantly from the circular muscle-to-longitudinal muscle transfer resistances. These observations indicate that there is an appreciable resistance between the compartment containing circular smooth muscle cells and the compartment containing

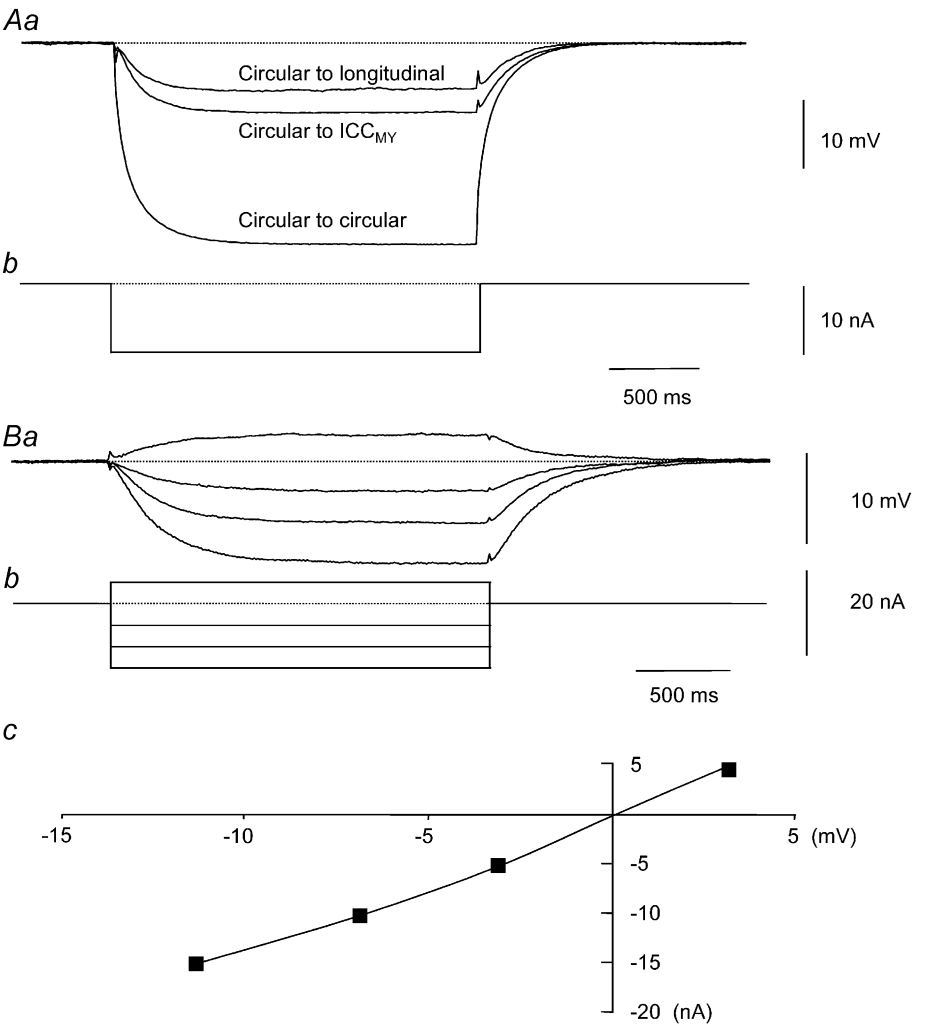

Figure 3. Electrical coupling between the three cell layers of the gastric antrum and the lack of rectification between ICC_{MY} and the circular muscle layer of the gastric antrum

Aa, electrotonic potentials recorded from the longitudinal, ICC_{MY} and circular layer, each produced by injecting current (*Ab*) into the circular layer in the interval between slow waves. In this experiment the membrane potentials of the circular smooth muscle layer, ICC_{MY} and longitudinal layer were −64, −63 and −62 mV, respectively. *B*, a family of electrotonic potentials (*Ba*) recorded from an ICC_{MY} generated by injection of hyperpolarizing and depolarizing currents (*Bb*) into a circular muscle cell. *Bc*, the relationship between injected current and membrane potential response was close to linear (see text). The membrane potentials of the circular smooth muscle layer and ICC_{MY} were −67 and −66 mV, respectively. The time bars apply to all traces.

ICC_{MY}, and that there is an appreciable resistance between the ICC_{MY} and longitudinal muscle compartments. The time courses of the electrotonic potentials also varied in a systematic manner; those recorded from the circular layer started abruptly with the onset of current flow (Fig. 3*Ab*), whereas those recorded from ICC_{MY} and the longitudinal layer each started after a brief electrotonic delay (Fig. 3*Aa*). When the circular layer was impaled with a current-passing electrode and the second electrode was used to record electrotonic potentials at various depths within the circular layer and at varying electrode separations, the amplitudes of electrotonic potentials recorded from different cells in the circular muscle layer of a given preparation varied by less than 5 %. These observations suggest that during the passage of a long pulse of current, the membrane potential throughout the circular layer is uniform. In three experiments, the two electrodes were placed in the longitudinal layer. In each of these cases, current injected into one electrode generated an electrotonic potential at the second recording electrode: this indicates that longitudinal muscle cells are electrically coupled to neighbouring cells (see Cousins *et al.* 1993).

Lack of rectification between ICC_{MY} and the circular muscle layer

Previous experiments have confirmed that ICC_{MY} are electrically coupled to both the circular (Dickens *et al.* 1999) and longitudinal muscle layers (Hirst & Edwards, 2001), but show that appreciable access resistances exist between the three layers. In the present experiments, hyperpolarizing or depolarizing currents passing into the circular layer caused hyperpolarizing and depolarizing electrotonic potentials in ICC_{MY} (Fig. 3*Ba*). Except when large hyperpolarizing currents were used, the relationship between hyperpolarizing and depolarizing membrane potential changes was linear (Fig. 3*Bc*). The deviations from linearity at more negative potentials appeared to result from changes in the resistance of the circular muscle layer rather than changes in the properties of the connections between the two layers. Thus, when the membrane potential of the circular layer was hyperpolarized beyond −80 mV, the muscle displayed inward rectification. When the relationship between amplitudes of electronic potentials in ICC_{MY} and electrotonic potentials in the circular layer was plotted, it was found to be linear for all currents injected. Unfortunately, it was not possible to examine the electrical properties of the connections between the circular layer and ICC_{MY} over more positive voltage ranges, as the electrodes invariably rectified, preventing the injection of large depolarizing currents. In three preparations, hyperpolarizing currents were passed into the circular layer and electrotonic potentials were detected in the longitudinal layer. Subsequently, the same current was injected into the longitudinal layer, and on each occasion a hyperpolarizing potential was detected in the circular layer. Clearly, for this to be the case the connections between ICC_{MY} and both adjacent muscle layers must have passed hyperpolarizing current in either direction. Together, the experiments suggest that the connections between the different cell layers do not rectify and the explanation for the ability of the three cell layers to generate different membrane potential changes during each slow wave cycle must have a different basis.

Variations in the electrical coupling between ICC_{MY} and the circular muscle layer

The transfer resistance between the circular layer and the layer of ICC_{MY} varied from preparation to preparation. A part of this variation arose because the input resistance of individual preparations varied, presumably because of differences in the sizes of the preparations. When this contribution was accounted for by determining the coupling ratio (i.e. the transfer resistance between the circular layer and ICC_{MY} divided by the input resistance of the preparation measured at the circular layer), the coupling ratio was again found to vary from preparation to preparation. This did not result simply from experimental error: the variations in coupling between different preparations were related to differences in the shapes of slow waves recorded from those preparations. Two sets of observations are illustrated in Fig. 4. In Fig. 4*A*, it can be seen that a pacemaker potential of 45 mV amplitude triggered a slow wave with an initial component of 10 mV and a peak amplitude of 35 mV. This preparation had a relatively low coupling ratio, since the electronic potential detected in the circular layer (Fig. 4*Bb*) was considerably larger than that detected in the ICC_{MY} (Fig. 4*Ba*). The next part of the figure (Fig. 4*C* and *D*) shows observations made from a separate preparation taken from the same animal. Although the pacemaker potentials and slow waves each had similar peak amplitudes to those shown in Fig. 4*A*, the initial component of the slow wave was much larger, being about 32 mV (Fig. 4*C*). In this preparation the coupling ratio was much higher, with the electronic potential detected in the circular layer (Fig. 4*Db*) being only slightly larger than that detected in the ICC_{MY} (Fig. 4*Da*). These observations and those made from the other experiments in which recordings were made from ICC_{MY} and the circular layer are summarized in Fig. 4*E*. It can be seen that the coupling ratio and the amplitude of the initial component of the slow waves varied in a linear manner, with the observations not differing significantly from the calculated straight line of best fit. When the amplitudes of pacemaker potentials were compared with the amplitudes of the initial component detected in the same preparation, no correlation was detected. These observations suggest that coupling between ICC_{MY} and the circular layer varies within the gastric antrum, and when good coupling exists, a larger proportion of the slow wave is generated by current flow from ICC_{MY}.

Estimation of coupling resistances between the muscle layers and ICC_{MY}

The properties of the coupling resistances between the muscle layers and the layer of ICC_{MY} were determined. To do this it was assumed that cells within each layer, longitudinal, circular and ICC_{MY}, are isopotential and can be represented as single lumped resistances (R_L, R_C and R_{ICC}, respectively; see Fig. 1*B*). The inclusion of a coupling resistance between the circular layer and ICC_{MY} network ($R_{C–IC}$) and a resistance between the longitudinal layer and ICC_{MY} network ($R_{L–IC}$) means that there are five unknown variables (Fig. 1*B*). The values of each unknown resistance could then be estimated if first a known current was injected into the longitudinal layer and the potential change it produced was determined in the longitudinal layer, in the ICC_{MY} network and in the circular layer. Second, the same current was injected into the circular layer and the potential change it produced could be determined in the circular layer, in the ICC_{MY} network and in the longitudinal layer. Unfortunately, we were only able to successfully complete such a series of measurements on one occasion. Analysis of these data gave values of 0.59, 2.58 and 3.97 MΩ for R_C, R_{ICC} and R_L, respectively. For the coupling resistances, the values were 1.11 and 1.3 MΩ for $R_{C–IC}$ and $R_{L–IC}$, respectively, suggesting that these two parameters are similar.

A simpler and experimentally feasible approach is to inject current into the circular layer and determine the amplitude of the electrotonic potential in the circular layer (Fig. 1*B*; V_1), the ICC_{MY} layer (V_2) and the longitudinal layer (V_3). Additional information about the network is then obtained by determining the amplitude of the pacemaker potential, which is generated by ICC_{MY} (Fig. 1*C*; V_5), and the amplitude of depolarization that it produced in the circular layer (i.e. the amplitude of the initial component of the slow wave, V_4). These measurements then allow one to determine values for R_L, R_C, R_{ICC}, $R_{C–IC}$ and $R_{L–IC}$, if one assumes that $R_{C–IC}$ and $R_{L–IC}$ have the same value (see Methods). Experimental observations from one experiment are shown in Fig. 5. It

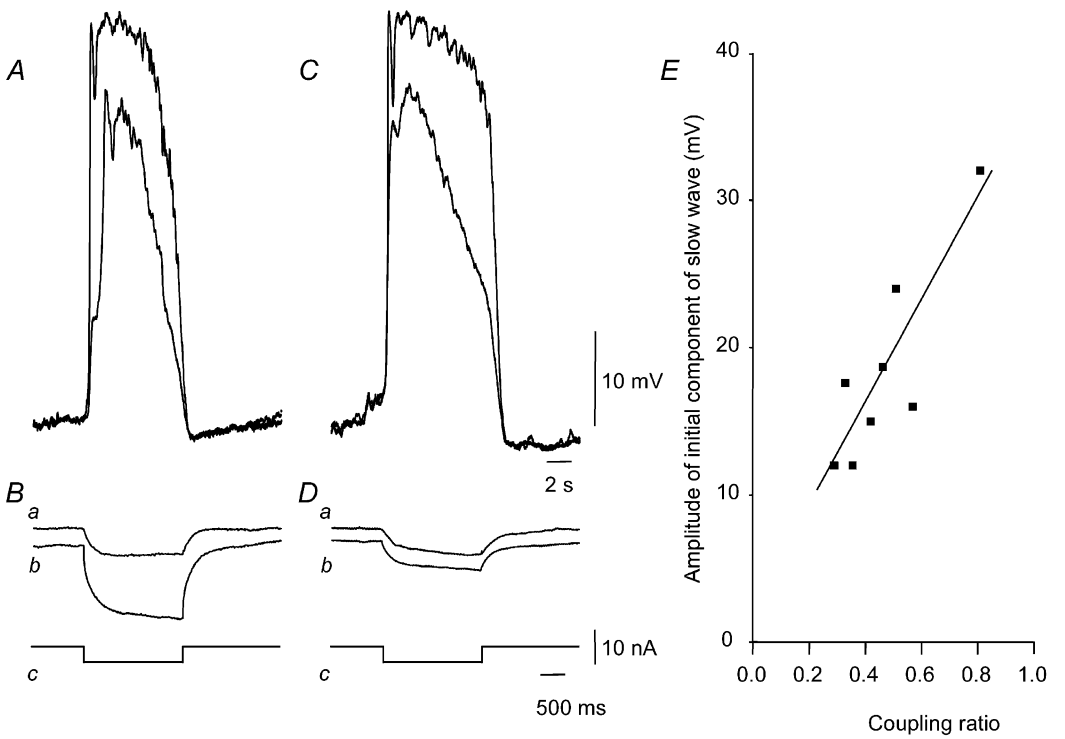

Figure 4. Variability in electrical coupling between ICC_{MY} and the circular muscle layer in different preparations

A, superimposed simultaneous membrane potential traces recorded from an ICC_{MY} and a circular muscle cell (smaller amplitude trace). Note the modest initial component of the slow wave. *B*, electrotonic potentials recorded from ICC_{MY} (*a*) and circular muscle (*b*) in response to current (*c*) injected into the circular muscle layer: the membrane potentials of the circular smooth muscle layer and ICC_{MY} were −60 and −62 mV, respectively. *C*, superimposed simultaneous membrane potential traces recorded from a different bundle obtained from the same animal. Note the large initial component of the slow wave. *D*, electrotonic potentials recorded from ICC_{MY} (*a*) and circular muscle (*b*) in response to current (*c*) injected into the circular muscle layer: the membrane potentials of the circular smooth muscle layer and ICC_{MY} were −63 and −63 mV, respectively. The voltage and current calibration bars apply to all traces. *E*, relationship between the coupling ratio (see text) and the amplitude of the initial component of the slow wave, together with a straight-line fit.

can be seen that when a pulse of current was injected into the circular layer it produced potential changes in the circular layer (Fig. 5*Ac*; V_1), ICC_{MY} network (Fig. 5*Bc*; V_2) and longitudinal layer (Fig. 5*Cc*; V_3). In this preparation the pacemaker potential had an amplitude of 42 mV (Fig. 5*Bb*; V_5), which produced an initial component of some 15 mV in the circular layer (Fig. 5*Bb*; V_4). Applying the simplified analysis to the data used for the previous unconstrained example gave values of 0.59, 3.03 and 4.92 MΩ for R_C, R_{ICC} and R_L, respectively. The coupling resistances R_{C-IC} and R_{L-IC} both took a value of 1.13 MΩ. The five equivalent resistor values derived by these two methods agree to a first approximation, the alternatives varying by less than 20 %.

The results from four experiments are included in Table 1. The four columns on the right of the table show the calculated resistance values divided by the value of R_C for each preparation. This was done to reduce dispersion due to differences in preparation size. Normalized mean values for resistors in the equivalent circuit were then 2, 12.3 and 9.3 MΩ for R_C, R_{ICC} and R_L, respectively, and 3.3 MΩ for coupling resistances R_{C-IC} and R_{L-IC}.

Together, the measurements and calculations support the view that the resistances between the three different layers of cells are high when compared to the resistances between cells in a given layer.

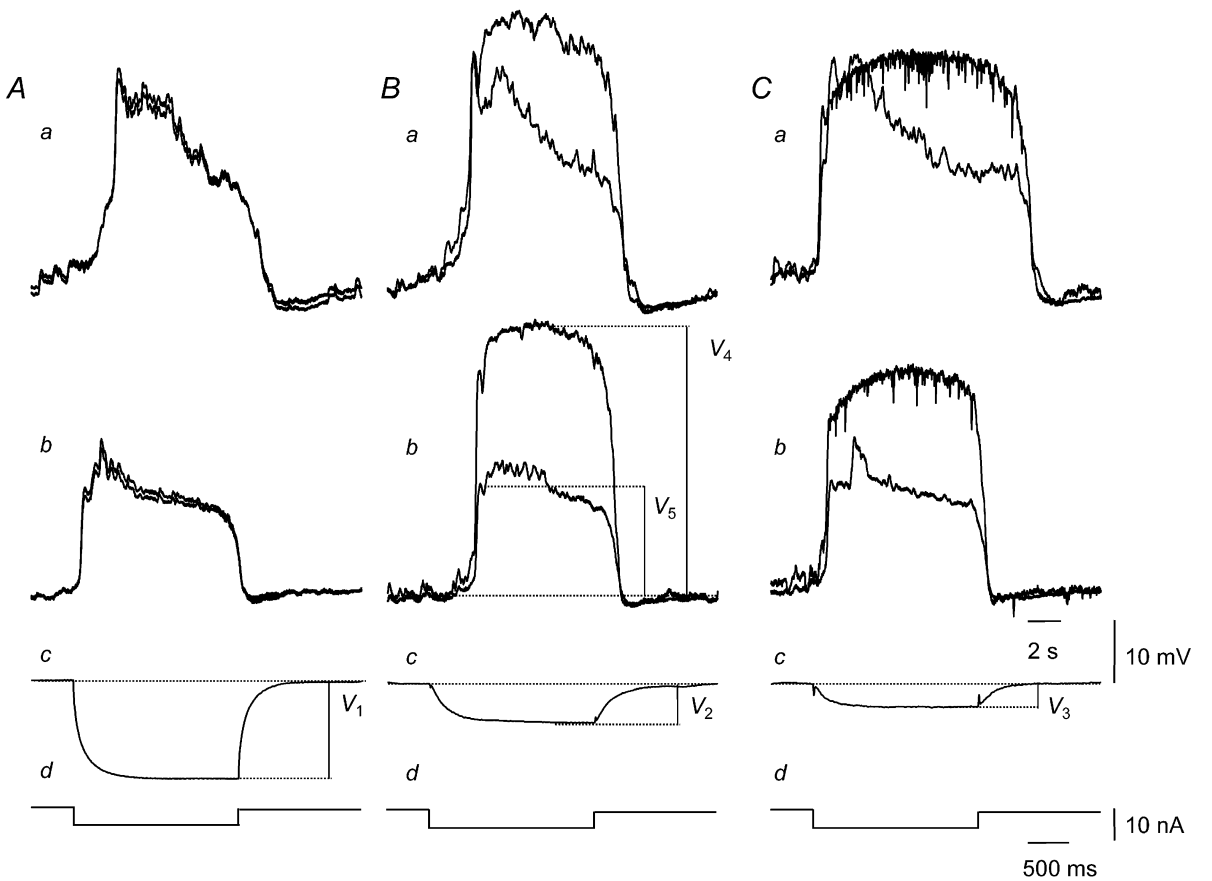

Figure 5. Calculation of coupling resistances between the ICC_{MY}, longitudinal and circular muscle layers

Aa, slow waves recorded simultaneously from two different points in the circular muscle layer. *Ab*, the waveforms 3 min after caffeine (1 mM) was added to the solution. Note that while the regenerative component of the slow wave was reduced, the amplitude of the initial component was little altered. *Ac*, the average of 20 electrotonic potential responses to current (5 nA, *Ad*) injected into the circular muscle layer. *B*, a slow wave recorded from the a circular muscle cell, and a pacemaker potential recorded from ICC_{MY}, in control conditions (*a*) and in the presence of caffeine (*b*). *C*, simultaneous recordings of a follower potential and a slow wave in control conditions (*a*) and in the presence of caffeine (*b*), recorded from the circular and longitudinal muscle layers, respectively. Examples of steady-state membrane potentials V_1–V_5 are illustrated in panels *Ac*, *Bc*, *Cc* and *Bb*, respectively. The voltage and current calibration bars apply to all traces. The membrane potentials of the circular smooth muscle layer, ICC_{MY} and longitudinal layer were −64, −65 and −59 mV, respectively.

Table 1. Equivalent circuit resistor values

Experiment number	R_C (MΩ)	$R_{C\text{-}IC}$ $R_{L\text{-}IC}$ (MΩ)	R_{ICC} (MΩ)	R_L (MΩ)	R_C/R_C	$R_{C\text{-}IC}/R_C$ $R_{L\text{-}IC}/R_C$	R_{ICC}/R_C	R_L/R_C
1	4.17	6.33	3.75	14.85	1.00	1.52	0.90	3.56
2	0.59	1.14	3.03	4.92	1.00	1.91	5.09	8.27
3	1.51	2.55	17.36	1.58	1.00	1.69	11.52	1.05
4	1.68	2.43	12.15	9.72	1.00	1.45	7.25	5.80
Mean	1.99	—	—	—	1.00	1.64	6.19	4.67
Normalized mean	1.99	3.27	12.30	9.28	—	—	—	—

Normalized mean values are calculated by multiplying the mean values in the four right-hand columns by the mean value for R_C.

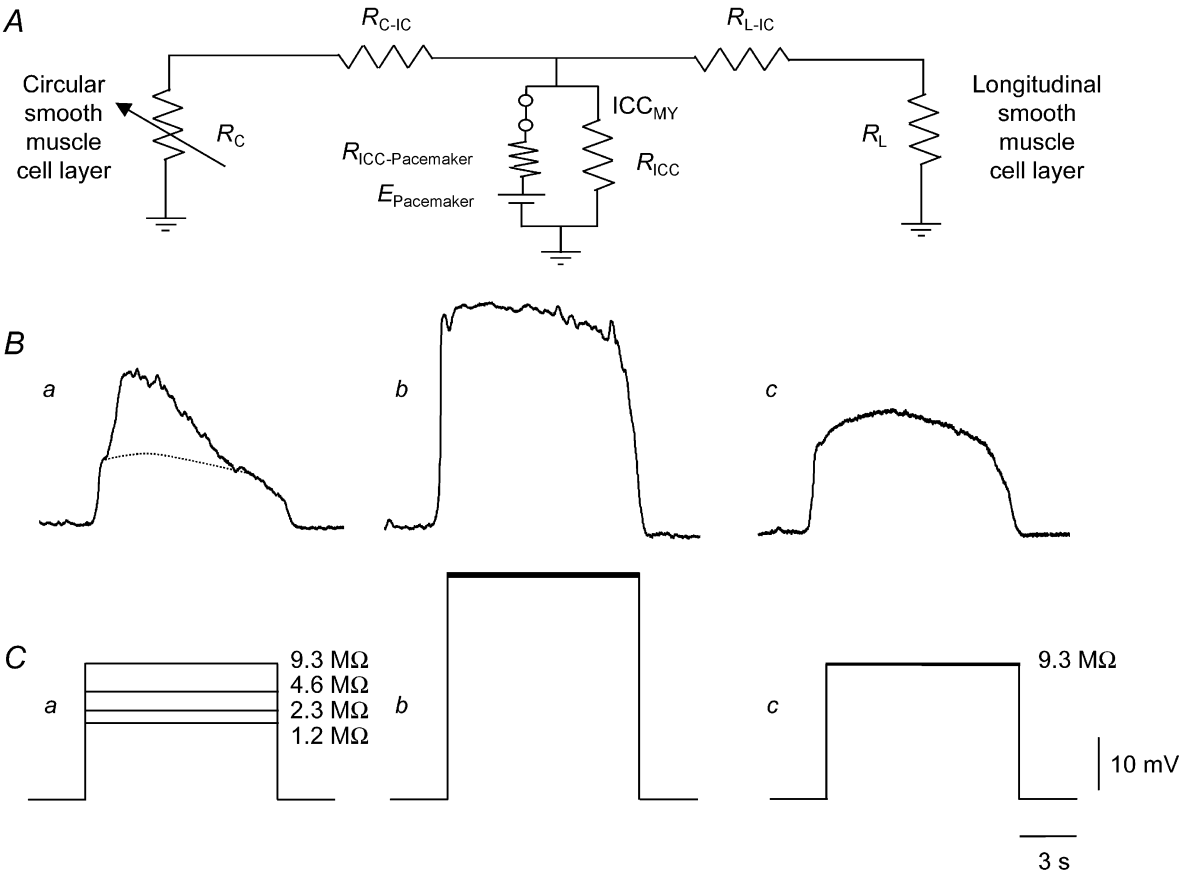

Figure 6. Asymmetrical membrane potential changes recorded from different cell types during the pacemaker cycle

A, the equivalent circuit for a small segment of antral wall. The circular muscle layer is shown as a variable resistor (R_C), initially being allotted the same value as the longitudinal muscle layer (R_L; 9.3 MΩ). This simulation illustrates the difference between a symmetrically loaded ICC_{MY} layer and a more realistic asymmetrically loaded one. *Ba*, a slow wave with an initial component of about 12 mV; the amplitude of the initial component, which was determined in the presence of caffeine, is shown as a dotted line. *Bb*, a 40 mV pacemaker potential recorded in the ICC_{MY} layer, which generated the initial component of the slow wave shown in *Ba*. *Bc*, a follower potential recorded in the longitudinal muscle layer. *C*, simulations of slow waves (*Ca*), pacemaker potentials (*Cb*) and follower potentials (*Cc*) for four different values of R_C (equal to R_L, $R_L/2$, $R_L/4$ and $R_L/8$; i.e. 9.3, 4.6, 2.3 and 1.2 MΩ, respectively). Note that large changes in R_C result in moderate changes to the amplitude of the initial component of the slow wave and negligible changes to the amplitudes of the pacemaker potential and the follower potential. The membrane potentials of the circular smooth muscle layer, ICC_{MY} and longitudinal layer were −64, −64 and −65 mV, respectively.

Explanations for the differences between the rhythmical potential changes detected in the longitudinal and circular muscle layers

The previous sections have shown that the three layers of cells making up the muscular wall of the gastric antrum are electrically coupled into an electrical syncytium. However, the observations suggest that appreciable resistances exist between the three layers. This section will examine whether these electrical properties can explain how each cell layer generates distinct electrical signals during the pacemaker cycle. To do this, mean experimental values were assigned to elements of the equivalent circuit shown in Figs 1 and 6*A*; thus R_C, R_{C-IC}, R_{ICC}, R_{L-IC} and R_L were assigned values of 2, 3.3, 12.3, 3.3 and 9.3 MΩ, respectively (Table 1). During a pacemaker potential, it has been shown that the plateau membrane potential change approaches the reversal potential for chloride ions, and the equilibrium potential for the pacemaker current ($E_{Pacemaker}$) was assigned a value of 45 mV (Hirst & Edwards, 2001; see also Kito *et al.* 2002). Firstly, the amplitudes of the initial component of the slow wave and the follower potential detected in an individual preparation differed significantly (Figs 2, 5 and 6). A series of calculations are compared with experimental observations in Fig. 6*C*. It can be seen that in the sample data, a slow wave with a peak amplitude of 30 mV had an initial component with an amplitude of some 12 mV (Fig 6*Ba*) was generated by a pacemaker potential with an amplitude of 40 mV (Fig. 6*Bb*), and this gave rise to a follower potential with an amplitude of 20 mV (Fig. 6*Bc*). When identical values were assigned to R_C and R_L (9.3 MΩ), the predicted passive waves of depolarization were identical in both layers (Fig. 6*Ca* and 6*Cc*). As the resistance of the circular compartment (R_C) was progressively halved, from 9.3 down to 1.2 MΩ, the amplitude of the electrotonic depolarization was reduced (Fig. 6*Ca*), causing little change in the amplitude of either the pacemaker potential (Fig. 6*Cb*) or the follower potential (Fig. 6*Cc*). This does not imply that the cells making up the circular compartment have lower passive membrane resistances; the same change will occur if the number of cells in the circular layer is increased. This is the case, since the circular muscle layer in the antrum is much thicker than the longitudinal layer.

This calculation suggests that although the signals detected in each layer have different amplitudes, they will have similar shapes (other than being smoothed by the membrane capacitance of the cells in each layer). This clearly is not the case (see Figs 2 and 5); follower potentials recorded from the longitudinal layer lack secondary components (Fig. 6*Bc*), whereas secondary components are readily detected during each slow wave (Fig. 6*Ba*). When a current pulse was injected into the circular layer during the interval between slow waves, it produced an electrotonic potential in the longitudinal layer but failed to do so when injected during a slow wave (Fig. 7*B*). This could have resulted from the increase in conductance of the circular layer associated with the regenerative component of the slow wave. However, this seems to be an unlikely explanation, as similar observations were made when the experiments were repeated in the presence of caffeine (1 mM). Under these conditions, the secondary component of the slow wave is abolished (Dickens *et al.* 1999). However, a current pulse injected into the circular layer during the remaining passive component of the slow wave also failed to produce an electrotonic potential in the longitudinal layer. One explanation might be that if the membrane resistance of ICC_{MY} fell to a low value during each pacemaker potential, the current normally passing between layers would dissipate through the ICC_{MY} membrane. In this case, the reduction of the ICC_{MY} membrane resistance to a sufficiently low value could isolate electrical events in the circular muscle layer from those in the longitudinal muscle layer.

The three calculations shown in Fig. 7*D* show the relationship between the amplitude of an electrotonic potential detected in the longitudinal layer, which was evoked by current injection into the circular layer, and a varying pacemaker shunt ($R_{ICC-Pacemaker}$; Fig. 7*Da*). The relationship between the amplitude of an electrotonic potential detected in ICC_{MY} and a varying pacemaker shunt is shown in Fig. 7*Db*, and that between the amplitude of the pacemaker potential detected in ICC_{MY} and a varying pacemaker shunt is shown in Fig. 7*Dc*. It can be seen that when the conductance occurring during a pacemaker potential is very high, the electrical shunt prevents communication between muscle layers, but as the pacemaker conductance falls, even quite slightly, an appreciable signal is transmitted between the muscle layers.

Distribution of Cx43 in the gastric antrum of guinea-pigs

When preparations were stained with an antibody to Kit, a network of Kit-positive cells was detected in the myenteric region, ICC_{MY}, and these cells often appeared as a bilayer. Kit-positive cells were also observed interspersed within the circular muscle cell layers: these cells were spindle shaped and ran parallel to the circular muscle fibres, as described previously for the morphology of ICC_{IM} (Fig. 8*A*; see also Burns *et al.* 1997). Very occasionally, Kit-positive cells were detected in the longitudinal layer (Fig. 8*A*). A number of different connexins have been identified in different regions of the gastrointestinal tract in a range of different species (Nakamura *et al.* 1998; Seki *et al.* 1998; Seki & Komuro, 2001; Wang & Daniel, 2001). In this study, antibodies to three connexins Cx40, Cx43 or Cx45, were applied. Only Cx43 immunostaining was detected within the wall of the gastric antrum. Given that positive immunostaining to Cx40 and Cx45 was observed in rat endocardium and in rat tail artery endothelial cells (Cx40), the lack of immunopositive deposits for either

connexin in the guinea-pig antrum suggests that these connexins are unlikely to be present in the gap junctions of this tissue. In contrast, strong, punctate Cx43 immunostaining was observed throughout almost the entire thickness of antral circular muscle in a homogeneous fashion, as has been described previously (Seki *et al.* 1998). The pattern of Cx43 immunostaining was dependent upon the orientation of the section: when the cryosection was cut parallel to the circular muscle fibres, each muscle cell was seen in longitudinal orientation and was outlined by a row of discrete fluorescent immunopositive deposits (Fig. 8*B*). Cx43 immunoreactivity was detected at the serosal surface of the longitudinal layer (not shown), but was rarely detected within the longitudinal muscle layer itself (Fig. 8*B*). When detected within the longitudinal muscle layer, Cx43

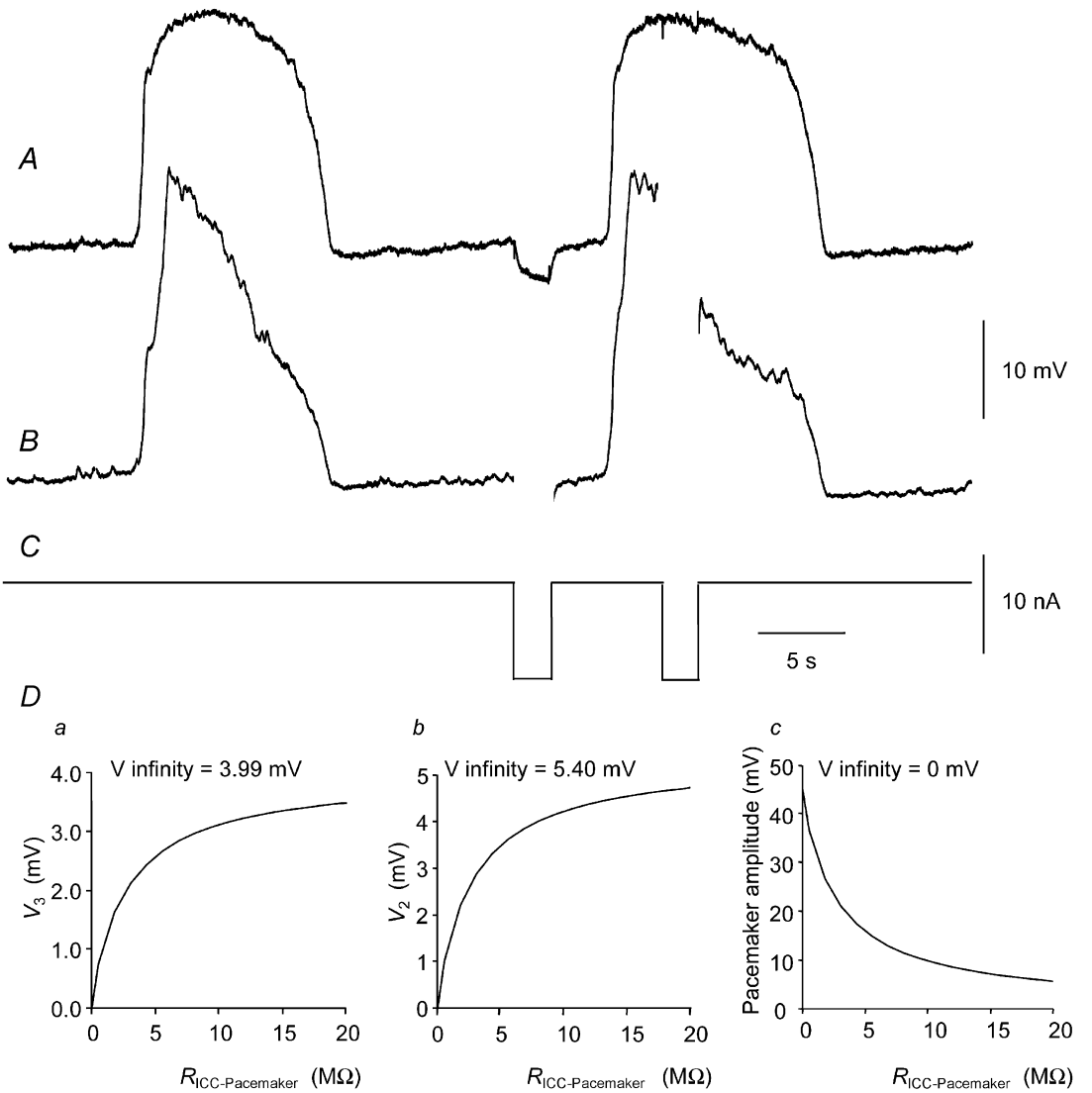

Figure 7. Electrical isolation of cell layers during a slow wave arises from changes in the membrane resistance of ICC_{MY} during each pacemaker potential

A, a successive pair of follower potentials. During the interval between slow waves, a current pulse (*C*) injected into the circular muscle layer (slow waves, *B*) generates an electrotonic potential in the longitudinal muscle layer. When the same current is injected near the peak of the slow wave, little or no electrotonic transmission is evident in the longitudinal layer. The voltage calibration bar applies to traces *A* and *B*. The time calibration bar applies to all traces. The membrane potentials of the circular smooth muscle layer and longitudinal layer were −62 and −61 mV, respectively. The apparent isolation of muscle cell layers during a slow wave can be explained if the membrane resistance of ICC_{MY} fell to a low value during the plateau component of each pacemaker potential. *Da*, the amplitude of the electrotonic response in longitudinal muscle as a function of pacemaker shunt resistance ($R_{ICC-Pacemaker}$, see Fig. 1). Injected current (I) was 5 nA and the values of R_G, R_{C-IC}, R_{ICC}, R_{L-IC} and R_L were 2, 3.3, 12.3, 3.3 and 9.3 MΩ, respectively, as before. *Db*, the amplitude of the electrotonic response in the ICC_{MY} layer as a function of $R_{ICC-Pacemaker}$. *Dc*, the amplitude of the pacemaker potential itself in the absence of injected current as a function of pacemaker shunt resistance.

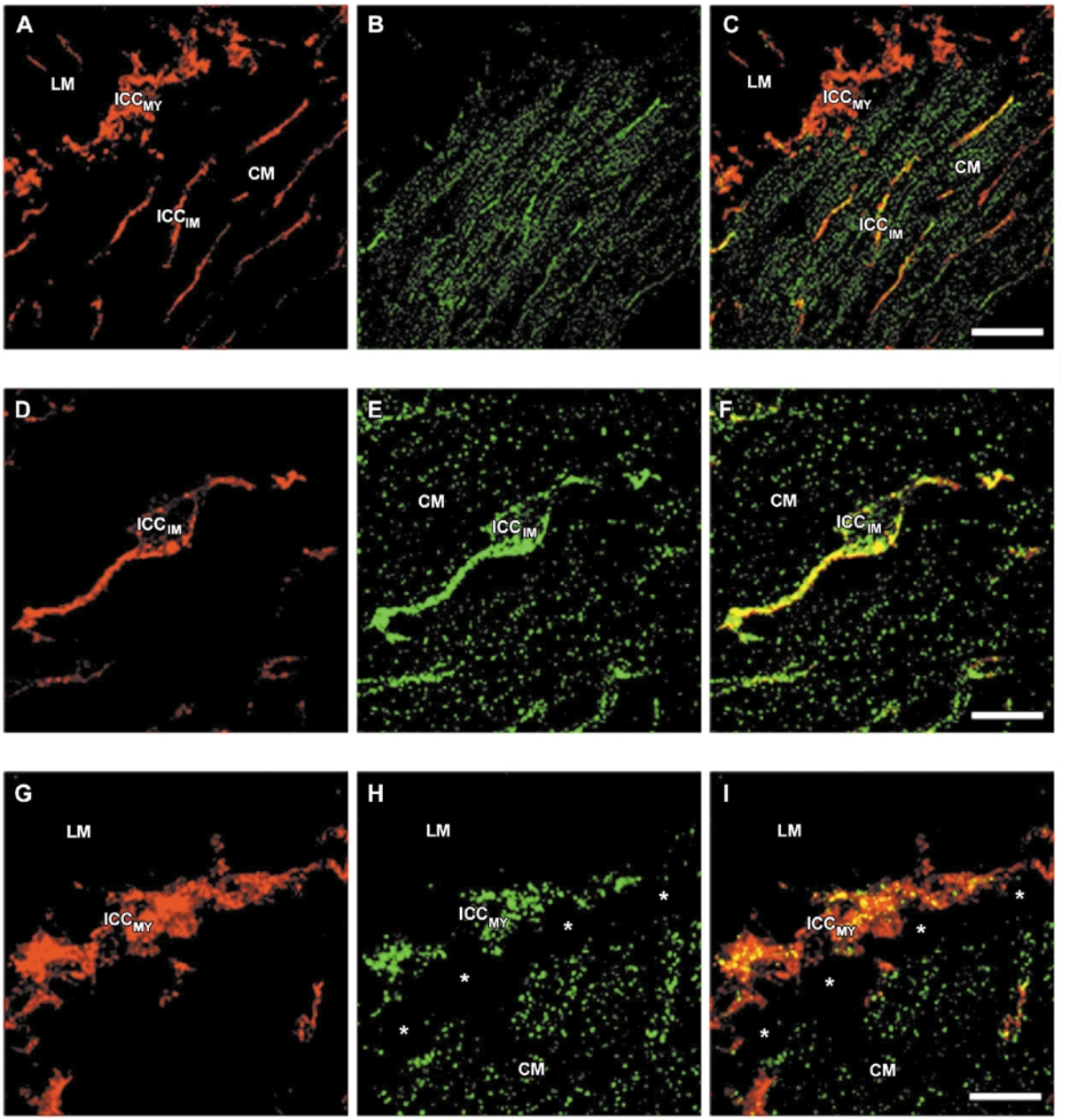

Figure 8. Distribution of Kit immunoreactivity and Cx43 immunoreactivity in muscular wall of the gastric antrum

A, *B* and *C*, a *Z*-stack of a transverse cryosections of the guinea-pig antrum immunostained for the Kit receptor, Cx43 and a merged image of *A* and *B*, respectively. *A*, immunopositive deposits in the myenteric region in ICC_{MY} and on ICC_{IM} within the circular smooth muscle layer. A few deposits are also found in the longitudinal muscle layer (LM). *B*, Cx43 staining in the circular smooth muscle layer and on both ICC_{MY} and ICC_{IM}. The Cx43 immunostaining appears as dots arranged in lines along the surface of the longitudinally sectioned circular smooth muscle cells (CM). No Cx43 staining was apparent in the longitudinal smooth muscle layer except in regions where Kit immunoreactivity was detected. *C*, regions of colocalization of Kit with Cx43 are labelled yellow. Scale bar = 10 μm. *D*, *E* and *F*, a *Z*-stack of an isolated ICC_{IM} in the surrounding circular muscle immunostained for Kit, Cx43 and a merged image of *D* and *E*, respectively. Note that the density of Cx43 immunostaining is significantly greater on the ICC_{IM} compared with the circular smooth muscle (*E* and *F*). Scale bar = 50 μm. *G*, *H* and *I*, high-power images of a *Z*-stack illustrating a layer of ICC_{MY} and adjacent circular smooth muscle immunolabelled for Kit, Cx43 and the merged image of *G* and *H*, respectively. Cx43 staining is present in both ICC_{MY} and in the circular smooth muscle. Note that there is a region that is obviously devoid of Cx43 immunostaining in the circular muscle immediately adjacent to the ICC_{MY} (*). Scale bar = 50 μm (*A*–*C*) or 10 μm (*D*–*I*).

immunoreactivity was colocalized with longitudinally positioned ICC (Fig. 8*C*). Cx43 immunostaining was also present on the surface of both ICC_{MY} and ICC_{IM} (Fig. 8*C*). The density of Cx43 immunostaining was higher on ICC_{IM} than in regions of circular muscle devoid of ICC_{IM} (Fig. 8*D–F*). In 41 preparations from six animals, where the number of smooth muscle cells present in each preparation was 27 ± 6 muscles per sample, the percentage of the surface area of smooth muscle membrane immunostained for Cx43 ranged from 0.8 to 1.9 % (0.9 ± 0.2 %, $n = 8$). In 16 preparations from eight animals, 22 individual ICC_{IM} were identified. The percentage of ICC_{IM} membrane associated with Cx43 immunoreactivity was found to lie in the range 1.3–13.5 % (9.5 ± 1.3 %, $n = 22$). Thus, the percentage area of smooth muscle cell membrane associated with Cx43 immunoreactivity differed significantly from that of ICC_{IM} membrane associated with Cx43 immunoreactivity. When the percentage of ICC_{MY} membrane associated with Cx43 immunoreactivity was determined in a similar way, it was found to lie in the range 2.7–19.1 % (7.6 ± 1.7 %, $n = 8$). In ICC_{MY}, the percentage area of membrane associated with Cx43 staining also differed significantly from that of smooth muscle cells. The percentage area of ICC_{IM} membrane covered with Cx43 immunoreactivity was not significantly different from that of Cx43 immunostaining of ICC_{MY}. When individual optical sections through the ICC_{MY} network were examined, it became apparent that the density of Cx43 immunopositive deposits in the circular muscle cell layer immediately adjacent to the ICC_{MY} was reduced compared with the density of Cx43 immunostaining in the remainder of the circular smooth muscle layer. This was also clear in some *Z*-stacks of optical sections (Fig. 8*G–I*). An estimate of the density of Cx43 immunopositive deposits in the circular layer immediately adjacent to ICC_{MY} was obtained by comparing the distance between the surface of an ICC_{MY} and the nearest Cx43 immunodeposit in the circular muscle layer with the distance of that same Cx43 immunopositive deposit with its nearest Cx43 immunopositive deposit in the circular muscle layer. The distance between the layer of ICC_{MY} and the nearest Cx43 immunopositive deposit in the circular muscle layer was 6.7 ± 0.2 μm, whereas the distance between Cx43 immunopositive deposits in the circular muscle layer was 1.6 ± 0.1 μm ($n = 6$, 13 preparations). This difference is statistically significant.

DISCUSSION

The experiments described herein show that the three layers of rhythmically active cells making up the muscular wall of the guinea-pig antrum are electrically coupled to form a syncytium. However, the coupling between cells in each layer is more efficient than it is between cells in adjacent layers. This allows ICC_{MY} to generate characteristic pacemaker potentials, despite their connections with the large electrical sinks provided by the two muscle layers, but still allows sufficient current flow to passively initiate rhythmical potential changes in the adjacent muscle layers. The immunohistochemical data suggest that the relatively poor coupling between ICC_{MY} and the circular layer arises because immediately adjacent to the layer of ICC_{MY}, the density of Cx43 immunopositive deposits is low.

Pacemaker potentials generated by ICC_{MY} initiate slow waves in the circular muscle layer (Dickens *et al.* 1999) and follower potentials in the longitudinal muscle layer (Hirst & Edwards, 2001). Thus, slow waves and follower potentials occurred synchronously in the present study, with pacemaker potentials triggering the depolarizations (Fig. 2). When current was injected into the circular layer, it produced membrane potential changes in the circular layer, ICC_{MY} and longitudinal muscle layer, indicating that all three layers are electrically coupled to form a syncytium. However, marked voltage gradients between the three layers of cells were detected (Fig. 3), indicating that appreciable resistances between compartments exist. Thus, a membrane potential change generated in one layer will give rise to an attenuated potential change in the adjacent layer. For example, waves of depolarization produced by ICC_{MY} will produce attenuated passive waves of depolarization in the adjacent muscle layers. In the circular layer, the pacemaker wave is augmented by the secondary component of the slow wave, which is generated by ICC_{IM} (Dickens *et al.* 2001; Hirst *et al.* 2002*a*). Together, the findings thus support the view that slow waves generated in the circular layer consist of passive initial and active secondary components (Ohba *et al.* 1975). The high resistances between the three cell compartments will also restrict the membrane potential changes produced by stimulating inhibitory and excitatory nerves largely to the compartment where the innervation density is highest. Thus, although there are many reports that suggest that ICC_{IM} in the circular layer are densely innervated by inhibitory nerves (Burns *et al.* 1996), there is little indication that either ICC_{MY} or the longitudinal layer receives inhibitory innervation (Toma *et al.* 1999). In the circular layer of the antrum, inhibitory nerve stimulation evokes a rapid apamin-sensitive inhibitory junction potential (IJP) and a smaller-amplitude nitrergic IJP (Dickens *et al.* 2000; Suzuki *et al.* 2003). However, only small-amplitude IJPs are detected in ICC_{MY}, and even more attenuated IJPs are detected in the longitudinal layer (Dickens *et al.* 2000). Similarly, cholinergic nerves innervate ICC_{IM} in the circular layer (Ward *et al.* 2000; Suzuki *et al.* 2003); when stimulated, they evoke large-amplitude regenerative responses (Hirst *et al.* 2002*b*). Under these circumstances, the depolarization detected in ICC_{MY}, although attenuated, is sufficient to trigger a premature pacemaker potential in the network of ICC_{MY} (Hirst *et al.* 2002*b*).

When the distribution of Cx43 immunopositive deposits was determined, they were found to be distributed widely throughout the circular layer, with individual ICC_{IM} having a high proportion of their membranes associated with Cx43 immunoreactivity (Fig. 8). These observations are consistent with previous ultrastructural observations showing that gap junctions between ICC_{IM} and nearby smooth muscle cells are readily detected (Seki *et al.* 1998). Together, these data suggest that individual ICC_{IM} are tightly connected electrically into the circular muscle layer. A high density of Cx43 immunoreactivity was also associated with ICC_{MY}, suggesting that ICC_{MY} form a well-coupled network of cells, an idea that is well supported by the experimental finding that injected neurobiotin readily diffuses through the ICC_{MY} network (Dickens *et al.* 1999), and by the frequent detection of gap junctions between ICC_{MY} (Jimenez *et al.* 1999). However, in the layer of circular smooth muscle cells immediately adjacent to ICC_{MY}, the density of Cx43 immunopositive deposits fell (Fig. 8*I*). The simplest explanation for our findings is that the high electrical resistance detected between the circular smooth muscle layer and the layer of ICC_{MY} arises because the density of gap junctions in this region is low. This suggestion is supported by ultrastructural observations indicating that although gap junctions can be readily detected between individual ICC_{MY}, they are only rarely detected between ICC_{MY} and nearby circular smooth muscle cells (Daniel & Wang, 1999; Jimenez *et al.* 1999). This argument would be more convincing if we had been able to detect a similar pattern of connexin distribution within the longitudinal layer and between it and ICC_{MY}. Even though functional studies clearly show that neighbouring longitudinal smooth muscle cells are electrically connected to neighbouring cells (Bolton, 1972; Cousins *et al.* 1993), several previous studies, like the present study, have failed to identify the anatomical structures that allow electrical coupling to occur (Daniel & Wang, 1999). Presumably the gap junctions in the longitudinal layer involve a different connexin to those of the circular layer, or alternatively the gap junctions are so small that they cannot be resolved by either our methods or the ultrastructural methods used previously.

The connections between layers showed neither time-dependent nor voltage-dependent rectification (Fig. 3). Thus, an explanation is required for the finding that the circular and longitudinal muscle layers generate different sequences of membrane potential changes during each slow-wave cycle (Figs 2 and 6). Our explanation is that during a pacemaker potential, the membrane resistance of ICC_{MY} falls to such a low value that it shunts to the extracellular space almost all of the current that would otherwise pass between layers. When the conditions under which this might occur were explored numerically, it was found that the membrane resistance of the ICC_{MY} would have to fall dramatically (Fig. 7), and when this occurred, the membrane potential of the ICC_{MY} would be very close to $E_{Pacemaker}$. This suggestion is in accordance with the view that during the plateau phase of the pacemaker potential, an increase in chloride conductance brings the membrane potential close to E_{Cl} (Hirst & Edwards, 2001; Kito *et al.* 2002). Alternatively, the membrane resistance of ICC_{MY} would fall to a very low value if each pacemaker potential was associated both with the flow of pacemaker current and a concurrent increase in potassium conductance; this seems unlikely as the membrane potential achieved during a pacemaker potential is little affected by changes in the external concentration of potassium ions (Kito *et al.* 2002).

In summary, these experiments have shown that in the guinea-pig antrum, ICC_{MY} are electrically connected to the adjacent longitudinal and circular muscle layers in a way that allows them to function as pacemaker cells in the gastrointestinal tract. This will occur simply because each pacemaker potential can adequately depolarize the adjacent muscle layers. In the longitudinal layer, where the electrical load is small, the voltage changes will have large enough amplitudes to activate L-type calcium channels. In the circular layer, where the load is larger, the voltage changes are large enough to activate the secondary regenerative component of the slow wave, which in turn carries the membrane potential of circular smooth muscle cells through the activation curve of L-type calcium channels.

REFERENCES

Bolton TB (1972). The depolarizing action of acetylcholine or carbachol in intestinal smooth muscle. *J Physiol* **220**, 647–671.

Burns AJ, Herbert TM, Ward SM & Sanders KM (1997). Interstitial cells of Cajal in the guinea-pig gastrointestinal tract as revealed by c-Kit. *Cell Tissue Res* **290**, 11–20.

Burns AJ, Lomax AE, Torihashi S, Sanders KM & Ward SM (1996). Interstitial cells of Cajal mediate inhibitory neurotransmission in the stomach. *Proc Nat Acad Sci U S A* **93**, 12008–12013.

Coppen SR, Dupont E, Rothery S & Severs NJ (1998). Connexin45 expression is preferentially associated with the ventricular conduction system in mouse and rat heart. *Circ Res* **82**, 232–243.

Cousins HM, Edwards FR, Hirst GDS & Wendt IR (1993). Cholinergic neuromuscular transmission in the longitudinal muscle of the guinea-pig ileum. *J Physiol* **471**, 61–86.

Daniel EE & Wang Y-F (1999). Gap junctions in intestinal smooth muscle and interstitial cells of Cajal. *Microsc Res Tech* **47**, 309–320.

Dickens EJ, Edwards FR & Hirst GDS (2000). Vagal inhibitory projections to rhythmically active cells in the antral region of guinea-pig stomach. *Am J Physiol Gastrointest Liver Physiol* **279**, G388–399.

Dickens EJ, Edwards FR & Hirst GDS (2001). Selective knockout of intramuscular interstitial cells reveals their role in the generation of slow waves in mouse stomach. *J Physiol* **531**, 827–833.

Dickens EJ, Hirst GDS & Tomita T (1999). Identification of rhythmically active cells in guinea-pig stomach. *J Physiol* **514**, 515–531.

Edwards FR, Hirst GDS & Suzuki H (1999). Unitary nature of regenerative potentials recorded from circular smooth muscle of guinea-pig antrum. *J Physiol* **519**, 235–250.

Hill CE, Rummery N, Hickey H & Sandow SL (2002). Heterogeneity in the distribution of vascular gap junctions and connexins: implications for function. *Clin Exp Pharmacol Physiol* **29**, 620–625.

Hirst GDS, Beckett EAH, Sanders KM & Ward SM (2002*a*). Regional variation in contribution of myenteric and intramuscular interstitial cells of Cajal to generation of slow waves in mouse gastric antrum. *J Physiol* **540**, 1003–1012.

Hirst GDS, Dickens EJ & Edwards FR (2002*b*). Pacemaker shift in the gastric antrum of guinea-pigs produced by excitatory vagal stimulation involves intramuscular interstitial cells. *J Physiol* **541**, 917–928.

Hirst GDS & Edwards FR (2001). Generation of slow waves in the antral region of guinea-pig stomach – a stochastic process. *J Physiol* **535**, 165–180.

Jimenez M, Borderies JR, Vergara P, Wang Y-F & Daniels EE (1999). Slow waves in circular muscle of porcine ileum: structural and electrophysiological studies. *Am J Physiol* **276**, G393–406.

Kito Y, Fukuta H & Suzuki H (2002). Components of pacemaker potentials recorded from the guinea pig stomach antrum. *Pflugers Arch* **445**, 202–217.

Nakamura K-I, Kuraoka A, Kawabuchi M & Shibata Y (1998). Specific localization of gap junction protein, connexin45, in the deep muscular plexus of dog and rat small intestine. *Cell Tissue Res* **292**, 487–494.

Ohba M, Sakamoto Y & Tomita T (1975). The slow wave in the circular muscle of the guinea-pig stomach. *J Physiol* **253**, 505–516.

Ordog T, Ward SM & Sanders KM (1999). Interstitial cells of Cajal generate electrical slow waves in the murine stomach. *J Physiol* **518**, 257–269.

Rummery NM, Hickey H, McGurk G & Hill CE (2002). Connexin37 is the major connexin expressed in the media of caudal artery. *Arterioscler Thromb Vasc Biol* **22**, 1427–1432.

Sanders KM (1996). A case for interstitial cells of Cajal as pacemakers and mediators of neurotransmission in the gastrointestinal tract. *Gastroenterology* **111**, 492–515.

Seki K & Komuro T (2001). Immunocytochemical demonstration of the gap junction proteins connexin 43 and connexin 45 in the musculature of the rat small intestine. *Cell Tissue Res* **306**, 417–422.

Seki K, Zhou D-S & Komuro T (1998). Immunohistochemical study of the c-kit expressing cells and connexin 43 in the guinea-pig digestive tract. *J Auton Nerv Syst* **68**, 182–187.

Suzuki H & Hirst GDS (1999). Regenerative potentials evoked in circular smooth muscle of the antral region of guinea-pig stomach. *J Physiol* **517**, 563–573.

Suzuki H, Ward SM, Bayguinov YR, Edwards FR & Hirst GDS (2003). Involvement of intramuscular interstitial cells in nitrergic inhibition in the mouse gastric antrum. *J Physiol* **546**, 751–763.

Toma H, Nakamura K, Emson PC & Kawabuchi M (1999). Immunohistochemical distribution of c-Kit positive cells and nitric oxide synthase-positive nerves in the guinea-pig small intestine. *J Auton Nerv Syst* **75**, 93–99.

Van Helden DF, Imtiaz MS, Nurgaliyeva K, Von Der Weid P & Dosen PJ (2000). Role of calcium stores and membrane voltage in the generation of slow wave action potentials in guinea-pig gastric pylorus. *J Physiol* **524**, 245–265.

Wang YF & Daniel EE (2001). Gap junctions in gastrointestinal muscle contain multiple connexins. *Am J Physiol Gatsrointest Liver Physiol* **281**, G533–543.

Ward SM, Beckett EA, Wang X, Baker F, Khoyi M & Sanders KM (2000). Interstitial cells of Cajal mediate cholinergic neurotransmission from enteric motor neurons. *J Neurosci* **20**, 1393–1403.

Ward SM, Burns AJ, Torihashi S & Sanders KM (1994). Mutation of the proto-oncogene c-kit blocks development of interstitial cells and electrical rhythmicity in murine intestine. *J Physiol* **480**, 91–97.

Acknowledgements

This project was supported by a grant from the Australian NH & MRC. We are grateful to Dr Narelle Bramich for her critical reading of the manuscript.